Desalination and Water Treatment
www.deswater.com

doi: 10.1080/19443994.2016.1190108

57 (2016) 26657–26669
November

Taylor & Francis
Taylor & Francis Group

Evaluation of forward osmosis membrane performance by using wastewater treatment plant effluents as feed solution

Gyeong-Wan Go[a], Sung-Ju Im[a], Sang-Hak Lee[b], Am Jang[a,*]

[a]*Graduate School of Water Resources, Sungkyunkwan University (SKKU), 2066, Seobu-ro, Jangan-gu, Suwon-si, Gyeonggi-do 16419, Republic of Korea, Tel. +82 31 290 7535; Fax: +82 31 290 7549; email: amjang@skku.edu (A. Jang)*
[b]*Huviswater corporation, 425-100 (Moknae-dong) 90, Sandan-ro 83beon-gol, Danwon-Gu, Ansan-si, Gyeonggi-do, Republic of Korea*

Received 23 December 2015; Accepted 29 December 2015

ABSTRACT

Currently, there is a growing emphasis on seawater desalination and wastewater reuse around the world. Reverse osmosis (RO) is typically used for both seawater desalination and wastewater reuse. As an alternative technology of RO, forward osmosis–reverse osmosis (FO–RO) hybrid system has recently attracted attention. To select suitable membrane and feed water for this process, the performance of forward osmosis (FO) membrane according to the types of membrane and feed water quality was evaluated in this study, including three types of FO membrane (membrane I/II/III) and three types of feed water (1st/2nd/3rd wastewater treatment plant effluents, WWTP Efs). Despite high structural parameter, membrane II showed the highest water permeability (5.37 LMH/bar) with highest water flux (around 27.1 LMH) using draw solution of 0.5 M NaCl (feed solution: 5 mM NaCl). In fouling test, there was severe water flux decline when 1st WWTP Ef was used as feed solution compared to the case when 2nd/3rd WWTP Efs was supplied. Membrane III showed higher fouling resistance due to its chemistry characteristic compared to membrane I or II. Due to complex feed water characteristics, FO reversibility was lower compared to that of a previous study. Therefore, to optimize FO–RO hybrid system, FO membrane performance should be tested with different membrane characteristics and feed water qualities to develop suitable cleaning or pretreatment method and strategy to increase the reversibility of membranes.

Keywords: Feed solution; Forward osmosis membrane (FO); Membrane fouling; Structural parameter; Water flux

1. Introduction

Seawater desalination and wastewater recycling or reuse are expected to take responsibility for future water systems in parallel with water quality satisfaction. Markets of desalination and water reuse has steadily increased [1,2] It is being highly estimated at technical and economic points [3]. In fact, these technologies play significant role in quenching water-related problems.

From the beginning of successful installation of reverse osmosis (RO) plants in the late 1960s, RO

*Corresponding author.

Presented at the 8th International Desalination Workshop (IDW) 2015, November 18–21, 2015, Jeju Island, Korea

membrane has been developed over the past 40 years. It is commonly applied worldwide for seawater desalination and wastewater reuse [4]. RO membrane has high selectivity for salt (monovalent and divalent ions). It can remove organic matter and pathogen, thus producing high-quality water. However, due to high operating pressure over the osmotic pressure of feed water, RO process inevitably demands high energy consumption and expensive equipment with high fouling propensity [1,5], which can increase the CAPEX and OPEX of plants. Despite effort to reduce cost associated with the production of water cost such as energy recovery device and the development of high permeable membrane as well as the optimization of process configuration, RO technology is still energy-intensive. Therefore, new alternative processes are needed to make breakthroughs.

As an alternative technology of pressure-driven membrane, osmotically driven membrane using forward osmosis (FO) has recently received attention in order to reduce energy consumption during the desalination process. Like RO membrane, FO membrane has high salt rejection ability with several advantages, such as high water recovery, high efficiency in salt rejection, low operating pressure, and low fouling propensity [6]. As a derivation technology coming from FO with osmotic dilution membrane process, forward osmosis–reverse osmosis (FO–RO) has been proposed by Cath research team [7] and gained wide interests in the last decades. In particular, FO–RO system is one of the most promising ones due to its low energy demand compared to RO [7–9]. In addition, by diluting seawater as draw solution with impaired water as feed solution before desalination, the FO–RO hybrid system is an exceptionally robust multi-barrier system for treatment of municipal wastewater. It can produce freshwater at low cost. In addition, it can make water resource's availability higher [7]. However, there are still some challenges before the commercialization of FO. Most FO-related studies have been conducted by using model foulants with exclusive choice of membrane (i.e. Hydration Technologies Innovations) [5,10–15]. These can raise doubt about the actual efficiency of FO membrane in real conditions. Prior to commercialization (or scale-up to pilot system), it is necessary to decide which stage effluent from wastewater treatment plant (WWTP) is appropriate for operating FO system. In addition, the characteristics of different types of FO membrane need to be determined. Therefore, the objective of this study was to compare membrane fouling phenomenon with three different FO membranes according to different types of feed solutions to provide basic knowledge about strategies to render FO–RO hybrid system sustainable and feasible in respect to types of membrane and feed solution.

2. Materials and methods

2.1. FO membranes and FO filtration apparatus

Three kinds of flat-sheet FO membranes were provided by different manufacturers. Two manufacturers other than Hydration Technology Innovations (HTI; Albany, OR, USA) provided membrane I and II. They did not specify membrane chemical materials. Those membrane were presumed to be manufactured by thin-film composite (TFC) polyamide supported by polysulfone and polyester substances. Membrane III was provided by HTI typically used in previous studies for FO test. This membrane is known to consist of cellulose triacetate layer with an embedded polyester mesh as support layer.

For FO filtration test, lab-scale cross-flow system was set up. Custom built flat and frame FO membrane cell in which FO membrane was located was used. Schematic diagram of the FO filtration setup is shown in Fig. 1. The flat and frame FO membrane cell consisted of two symmetric channels (77 mm long, 26 mm wide, 3 mm deep) with a membrane effective area of 20.02 cm^2. The flow rate supplied into FO membrane cell was controlled by gear pumps (Longer Pump WT3000–1FA, China) for feed and draw side, respectively. The gear pump's flow rate was calibrated after filtration test to prevent flow rate change. A magnetic stirrer was used to equilibrate ionic strength in the feed tank. A chiller (CPT Inc., Korea) kept tanks' temperature constant at 25°C. A digital balance (AND GF-6000, USA) located under the draw solution tank was used to check weight change. It was connected to a computer to calculate water flux.

2.2. Methodology for the determination of transport and structural parameters

Transport and structural parameter were determined using a method recommended by the Elimelech research team [16]. Briefly, the experiment were performed in four stages. In the first stage, sodium chloride (NaCl) solution and deionized (DI) water were prepared as draw and feed solution. Water and solute flux were measured. The other three stages were performed in a similar fashion while draw solution concentration was increased as the stage was stepped up. The only difference was that feed water was changed after the end of each stage. However, the feed water was not changed. Its ionic strength was increased as

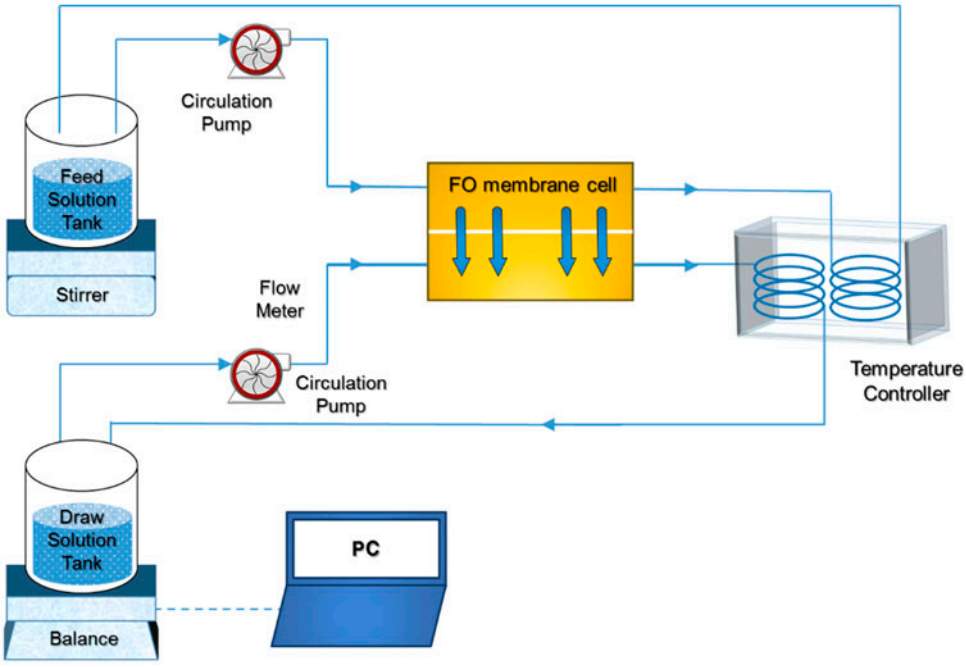

Fig. 1. Schematic diagram of the FO filtration setup.

the stage was stepped up. Based on the measurements of water and solute fluxes, transport and structure parameters were calculated by using an excel spreadsheet (Visual Basic) suggested by the Elimelech research team [16].

2.3. Feed and draw solutions

The feed solution was real wastewater treatment plant effluents (WWTP Efs). WWTP Efs were collected from local WWTP located in Suwon, Korea. It was stored at 4℃ before use. A flow diagram of each WWTP effluent used as feed water for FO filtration test is shown in Fig. 2.

The 1st WWTP Ef was filtered through 5 μm cartridge filter to remove easily settled particles and stabilize raw wastewater's concentration. Detailed characteristics of WWTP Efs is discussed in Section 3.2. The draw solution was 0.5 M NaCl solution prepared from sodium chloride (Samchun chemicals, Korea). NaCl solution at 5 mM was used to adjust ionic strength of the feed solution according to real WWTP Ef when baseline test was progressed.

2.4. Membrane baseline and fouling protocol

FO membrane is driven by osmotic pressure (chemical potential) difference between feed and draw solution as the water in the feed side flow into the draw

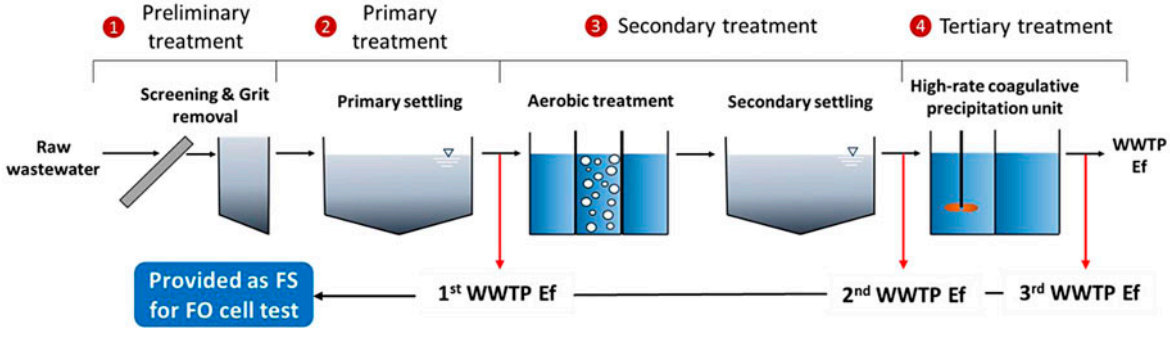

Fig. 2. Flow diagram of each WWTP effluent used as feed water for FO filtration test.

side across the membrane. As the permeate inflows, the draw solution is diluted and the osmotic pressure difference is decreased, thus decreasing the water flux. The extent of water flux decline induced dilution effect is dissimilar to the type of membranes due to different intrinsic transport parameters, different water and solute permeability (A and B), and different structural parameter (S). To prevent confusion induced by dilution effect and gain additional insights on the transport mechanism in FO system [13], baseline tests were performed. For all FO filtration tests, active layer faced the feed side (AL-facing-FS) based on FO mode. No spacer on either side was used in this experiment. Water flux was monitored with a digital balance and recorded in real time. To stabilize water permeate, water flux of the initial 15 min was discarded. Initial volumes of feed and draw solutions were 2 and 1 L, respectively. The conductivity of the feed solution was measured at predetermined time intervals using a conductivity meter to determine solute flux. Unless otherwise defined, the following operation conditions were used for both baseline and fouling test: 8.55 cm/s of cross-flow velocity for both sides; 25˚C of operating temperature; duration of base and fouling test (time for 500 mL of permeate produced).

In the fouling test, after 500-mL permeate was produced, solutions at both sides were replaced with new ones for consecutive fouling test. As the end of the second filtration test, physical cleaning was conducted using DI water to evaluate FO membrane reversibility. For the physical cleaning, 1 L DI water was circulated at both sides with 25.65 cm/s cross-flow velocity for 30 min. After the physical cleaning, a new set of fouling test was proceeded.

2.5. Calculation of water flux (J_w) and solute flux (J_s)

Water and reverse salt flux (RSF) were determined using the following equations:

$$J_{\mathrm{w}} = \frac{V_{t,2} - V_{t,1}}{At} \tag{1}$$

$$J_{\mathrm{s}} = \frac{C_t V_t - C_{\mathrm{o}} V_{\mathrm{o}}}{At} \tag{2}$$

where J_{w} was the water flux of a membrane (L/m^2/h), J_{s} was the RSF of a membrane (mmol/m^2/h), V_t was the volume of draw tank at time t, V_{o} was the volume of draw tank at time 0, C_t was the concentration of the draw solute in the feed tank at time t, C_{o} was the concentration of the draw solute in the feed tank at time 0, A was the membrane area (m^2), and t was operating time. The concentration of the draw solute in the feed tank was determined using predetermined calibration curve of NaCl. The conductivity was measured and converted to NaCl concentration.

2.6. Measurements

2.6.1. Solution characteristics

pH meter (Professional Plus, YSI, USA) and conductivity meter (Orion 4 Star, Thermo Scientific, USA) were used to measure pH and conductivity in the solution. Chemical oxygen demand and total organic carbon were measured using a water testing kit and spectrophotometer (Hach, DR 6000, USA) and TOC analyzer (TOC-L, Shimadzu, Japan). UV absorbance at 254 nm was measured with a spectrophotometer (DR 6000, HACH, USA). A fluorescence spectrophotometer (Shimadzu, Spectrofluorophotometer RF-5301pc, Japan) was used to identify organic components in WWTP Efs using a 1 cm cuvette. The DOC concentrations in WWTP Efs were diluted and adjusted to 1 mg/L for comparison of EEMs among samples. Ultrapure water's EEM was used to subtract a roman scatter peaks from that of other samples. For every FEEM measurement, roman scattering peak of ultrapure water was measured.

2.6.2. Characterization of virgin membrane

To identify virgin membrane characteristics, FESEM/EDX (JSM-7600F, JEOL, Japan) and FTIR (Bruker IFS-66/S, Bruker, Germany) analysis were performed. The EDX was equipped with FESEM to analyze elements and their relative compositions in the virgin membrane. The voltage used for the measurement was 15 kV (resolution: 1.0 nm) which provided high spatial resolution. The magnification was adjusted at both 500–5,000 times. The working distance was 8.0 mm. To identify functional group characteristics of the virgin membrane, FTIR measurement was performed using attenuated total reflection (ATR). The resolution of the ATR-FTIR spectrometer was better than 0.1 cm^{-1}. The wavenumber accuracy was 0.01 cm^{-1} with a scan rate of 110 scans/s.

3. Results and discussion

3.1. Membrane characterization

3.1.1. SEM/EDX and ATR-FTIR analyses

SEM/EDX and ATR-FTIR analyses were performed to identify the morphology, element compositions, and

functional groups of all three membrane. SEM images of the three virgin membranes (membrane I/II/III) are shown in Fig. 3. The typical feature of the TFC membrane is that its active layer has a ridge-and-valley structure (Fig. 3(a) and (b)). In contrast, membrane III showed a smoother surface (Fig. 3(c) and (d)). Membrane III is known to have lower mean roughness (~36 nm) compared to typical polyamide RO or FO membranes (~105 nm) based on AFM measurements [13,17–19]. Despite its higher mean roughness which is prone to be fouled, TFC membrane with innovative modification in the support layer structure can have better performance in respect to water flux and salt rejection as well as chemical resistance in FO process [20].

FO membrane belongs to salt-rejecting membrane as in nanofiltration and RO. In FO transport mechanism, internal concentration polarization (ICP) phenomenon induced by support layer is known to be able to significantly influence water and solute transport mechanism [14]. However, the active layer of membrane also plays a significant role in deciding water and solute flux [21]. Thus, it is important to know the characterization of membrane's active layer. ATR-FTIR technique is a useful method to identify the relative amounts of polymeric species by detecting functional groups of the material. This method has been widely applied in the membrane research area to determine foulants and modification of the membrane [22,23]. Therefore, ATR-FTIR measurement was performed to compare the chemical compositions among the three membranes. The ATR-FTIR spectrum for the three virgin membranes was in the range of 800–2,000 cm^{-1} (Fig. 4). The spectrum of membrane III showed peaks at wavenumber of 1,034 cm^{-1} (C–O), 1,215 cm^{-1} (C–C–O), and 1,738 cm^{-1} (C=O), which were reported in a similar fashion in a previous study [24]. As mentioned earlier, membrane I and II were thought to be polyamide. The spectrum of membrane I and II showed typical polyamide (active layer) peaks at wavenumber 1,650 and 1,541 cm^{-1}, indicating amide function group 1 (a primary amine, C–N=O) and group 2 (a secondary amine, C–N–H), respectively. In addition, membrane I and II showed polysulfone (support layer) peaks corresponding to wavenumber of 1,487, 1,503, and 1,584 cm^{-1} [22]. Therefore, these two

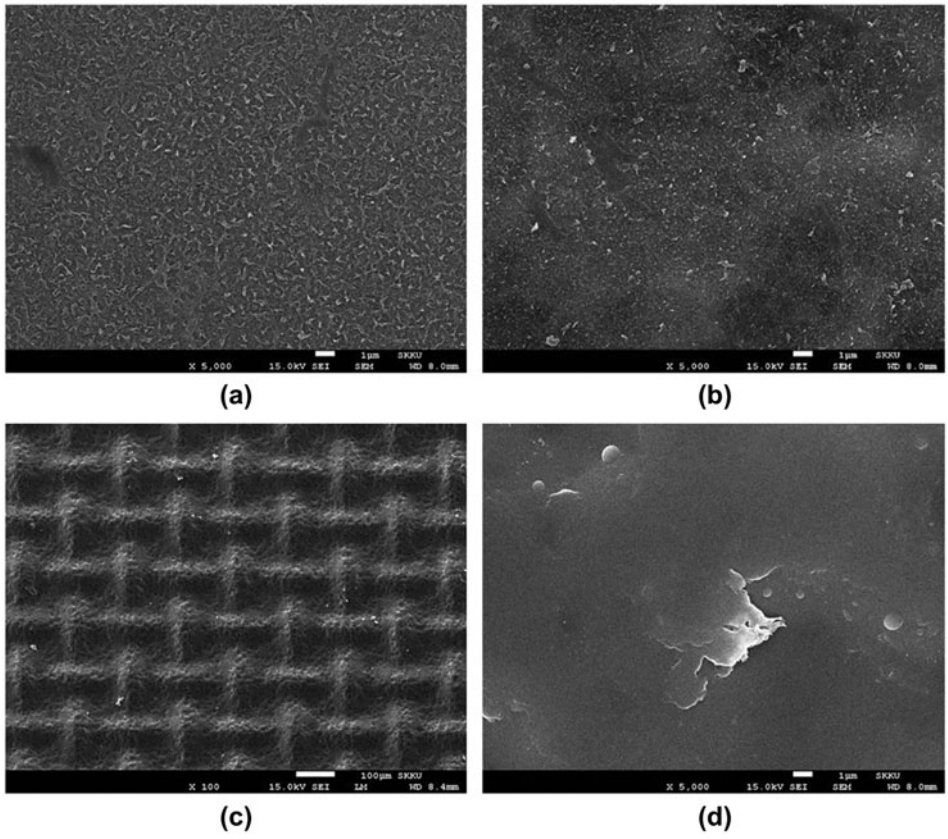

Fig. 3. SEM micrographs of virgin membrane I (a), membrane II (b), and membrane III (c and d). Magnification of 5,000 times for (a), (b), and (d) or 100 times for (c).

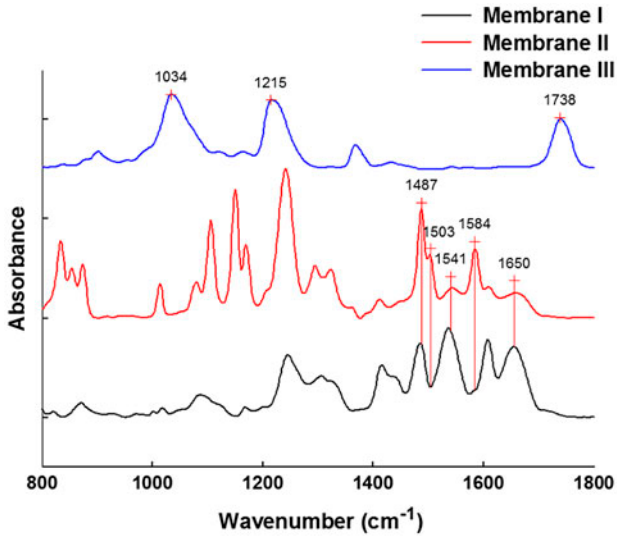

Fig. 4. ATR–FTIR spectrum of the three virgin membranes I, II, and III in the range of 800–1,800 cm^{-1}.

membranes are confirmed as PA-based ones. As expected, active and support layers of membrane I and II consisted of the same materials (polyamide and polysulfone) that their spectrum showed the same trend. Although their spectrums looked similar, they were clearly different in the intensity of absorbance. To compare the relative compositions between membrane I and II, the ratio of active to support layer was compared. Wavenumber 1,584–1,650 cm^{-1} corresponding to active and support layers were chosen based on previous study [22]. Compared to membrane II, membrane I had a higher height ratio at I_{1650}/I_{1584} of 2.593 compared to that of membrane II at 0.351. Within the framework of solution-diffusion model, water permeability is inversely associated with nonporous membrane active layer's thickness (l) since porous support layer has tiny impact on a transport mechanism [21]. Therefore, our results indirectly suggested that the active layer of membrane I was thicker than that of membrane II and that the water permeability of membrane I might be smaller than that of membrane II. This opinion will be discussed again in Section 3.1.2 (Table 1).

3.1.2. Transport and structural parameters of FO membranes

Transport and structural parameters were determined to identify the FO performance in the operating range of the FO–RO hybrid system. Results are summarized in Table 1. Based on a previous study, to lower the CAPEX and attain economic feasibility, the water flux is the most important variable in the FO–RO hybrid system [9]. FO membrane with higher water permeability (A >5 LMH/bar) and lower structural parameter (S < 100 μm) is preferred for economic feasibility [9]. Water permeability is determined by characteristic of membrane's active layer, while the structural parameter is determined by the characteristic of the membrane's support layer. Water permeability and ICP developed in the support layer can significantly affect water flux. Thus, it is essential to optimize the membrane's active and support layers to maximize the performance of FO membrane. Based on our results, membrane III showed the lowest water permeability with the highest structural parameter among the three membranes. As expected, it had the lowest water flux (9 LMH) in baseline test. In contrast, membrane I had the highest water permeability while membrane II had the lowest structural parameter. These membranes were expected to have better performance than membrane III. Considering the configuration of FO–RO hybrid system, the FO process was placed before RO process to lower the osmotic pressure. In this configuration, seawater was supplied for FO membrane as draw solution. Assuming that the osmotic pressure of feed water could be ignored, the osmotic pressure difference between the feed solution and the draw solution was around 25 bar. As a result of baseline test, despite its higher structural parameter, membrane II had water flux at around 28 LMH, while membrane I had water flux at 18 LMH (Fig. 6). Based on water flux, membrane II appeared to be more suitable and feasible than the other two.

3.2. Feed solution characterization

3.2.1. Primary properties of WWTP Ef

The primary properties of WWTP Efs are summarized in Table 2. As the treatment level was stepped up, the quality of WWTP Ef was improved. After the raw wastewater was treated by biological process, the values of COD, DOC, and UV254 were dramatically decreased.

3.2.2. FEEM analysis

With high sensitivity and selectivity, fluorescence spectroscopy has been applied as monitoring and foulants identification tool [25,26]. To obtain data on which components were in WWTP Ef, FEEM analysis was performed. The EEMs for the WWTP Efs are depicted in Fig. 5. FEEM matrix can be divided into

Table 1
Calculated parameters (A, B, and S) for the three membranes

Membrane type	Water permeability A (LMH/bar)	Solute permeability B (LMH)	Structural parameter S (μm)
Membrane I	1.27	0.944	70.6
Membrane II	5.37	0.961	235
Membrane III	0.818	0.618	334

Table 2
Primary properties of each WWTP Ef

Content	1st WWTP Ef	2nd WWTP Ef	3rd WWTP Ef
COD (mg/L)	129 (filtered w/5 μm)	15	10
DOC (mg/L)	27.20	4.58	4.96
UV_{254} (cm^{-1})	0.454	0.106	0.101
Conductivity (μS/cm)	667	488	510
pH	6.74	6.57	6.87

Notes: Values of the loadings chosen as proposed by B4 Method.

five regions. The corresponding excitation/emission wavelength and substances are as follows [27]:

(1) Region I, II: Ex/Em < 250 nm/< 350 nm, aromatic protein.
(2) Region III: Ex/Em <250 nm/> 350 nm, fulvic acid-like materials.
(3) Region IV: Ex/Em 250–280 nm/< 380 nm, soluble microbial by-product-like.
(4) Region V: Ex/Em > 280 nm/> 380 nm, humic acid-like organics.

As seen in Fig. 5, all WWTP Efs contained aromatic protein, fulvic acid-like materials, soluble microbial by-product-like (SMP), and humic acid-like organics. No distinct differences in WWTP Efs' characteristics were found among stages. However, the intensities of region I, II, and IV were increased in 2nd/3rd WWTP Efs compared to that of 1st WWTP Ef. The part of the fractions contained in 1st WWTP Ef might be non-detectable substances by FEEM measurements. The existing substances in WWTP 1st might be converted into detectable one by going through biological process (microbiological activity). SMP and aromatic protein had dominant percentage of the fluorescence in WWTP Efs as reported in a previous study [28]. Based on this result, the fouling mechanism might be different due to the transition of WWTP Ef characteristics.

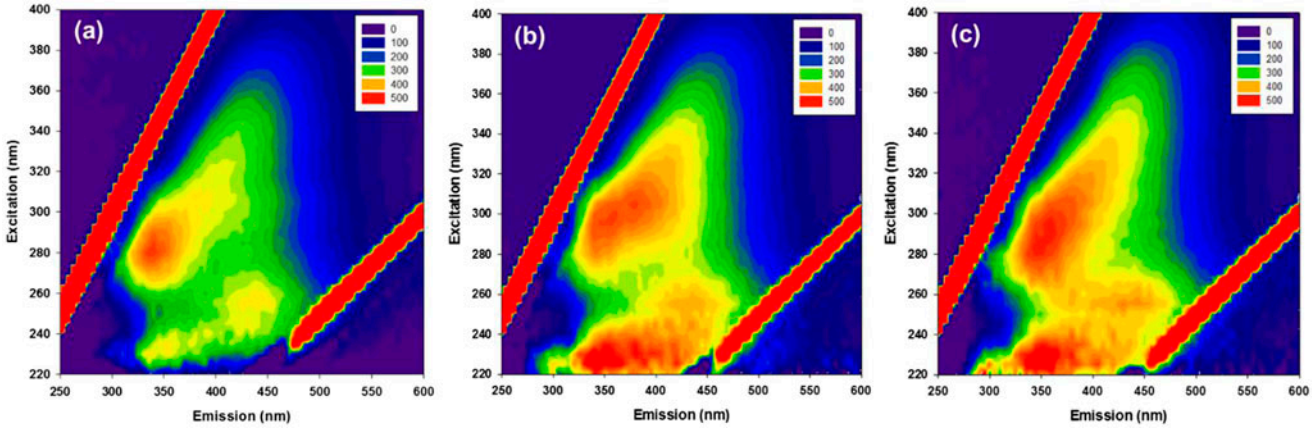

Fig. 5. EEMs of all WWTP Efs. (a), (b), (c) 1st, 2nd, and 3rd WWTP Ef, respectively (Normalized to 1 mg/L C).

3.3. FO cell test

3.3.1. Baseline test

In the FO process, draw solution was diluted as feed water was permeated through FO membrane to the draw solution side. FO permeate can decrease under no foulants condition due to dilution effect, causing confusion between fouling and FO permeate reduction when fouling test is performed [13]. To distinguish the two, prior to fouling test, baseline test was performed to determine whether the extent of permeate reduction was from the dilution effect. The water flux decline curves vs. volume of permeate for the three membranes are shown in Fig. 6. The x-axis was in unit of volume to compare water fluxes among membranes at the same level of dilution factor and to equalize the amount of convective particle moving toward the membrane. This can be used to compare fouling resistance among membranes with different initial water fluxes [29]. All three membrane showed different initial water flux (membrane II > I > III) with declining slopes. The driving force (osmotic pressure) can be hindered by several phenomena such as ICP, external concentration polarization, and reverse salt diffusion in the FO process [9,30]. These major phenomena are greatly associated with transport and structural parameters, which is why the three membranes used in this experiment have different declining slopes of water flux. When the water flux decline is compared among membranes with different intrinsic parameters, plotting by a normalized flux (J_w/J_o, here J_o: initial water flux) along the Y-axis can cause erroneous interpretation. This is why flux unit (J_w: LMH) is plotted along the Y-axis, not a dimensionless unit (normalized flux: J_w/J_o), in all articles.

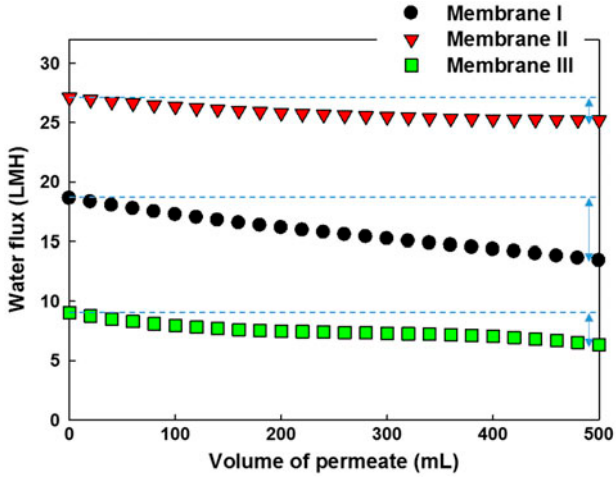

Fig. 6. Water flux (J_w) decline curve for membrane I/II/III in baseline test.

3.3.2. Fouling test

The water flux decline curves for 1st, 2nd, and 3rd WWTP Efs are shown in Figs. 7–9, respectively. As shown in Table 2, the fouling potential of 1st WWTP Ef was the highest. The water flux decline for the 1st WWTP Ef was the most remarkable one compared to that of the other two (2nd and 3rd WWTP Efs).

3.3.2.1. 1st WWTP Ef. In Fig. 7, compared to baseline, the foulants contained in the 1st WWTP Ef caused severe water flux decline in both membrane I and II. Different from other research studies that used model foulants as feed water, real WWTP Ef was used in this experiment. It is known that complex feed water can cause various fouling [31], including organic, inorganic, particulate, and biological fouling. In addition, the mechanisms of water flux decline in the FO process is known to be more complicated due to ICP and RSF than that in the pressure-driven membrane process [5,13]. Because of this convoluted situation in the identification of fouling mechanism, it is hard to clearly understand the fouling phenomenon. Thus, we focused on which membrane had greater fouling resistance and discussed the possible reason why that happened in this experiment. It is commonly known that lower initial flux and membrane roughness can reduce the extent of fouling in both pressure-driven and osmotically driven membranes [13,32–35]. In line with previous studies, membrane III showed the lowest fouling propensity without apparent flux reduction while membrane I and II showed higher initial water flux (membrane I: 18.6 LMH; membrane II: 27.1 LMH; membrane III: 9.1 LMH). The higher the initial flux is, the larger hydrodynamic drag force toward membrane and the higher concentration of polarization and compaction will be [23]. We can also concatenate this phenomenon with the critical flux concept developed by Field and coworkers which was first applied for microfiltration [36]. A range of applications using salt-rejecting membranes have used this concept, such as RO, NF, and FO [13,37,38]. According to the critical flux concept, under the condition when the initial water flux is above the critical flux, foulants will start to deposit on membrane surface and water flux will start to decline. In the critical flux concept, the foulant-membrane interaction can significantly affect the critical flux [39,40]. In addition, the chemistry characteristics (roughness, membrane morphology, pore size and zeta potential) of membrane's active layer can

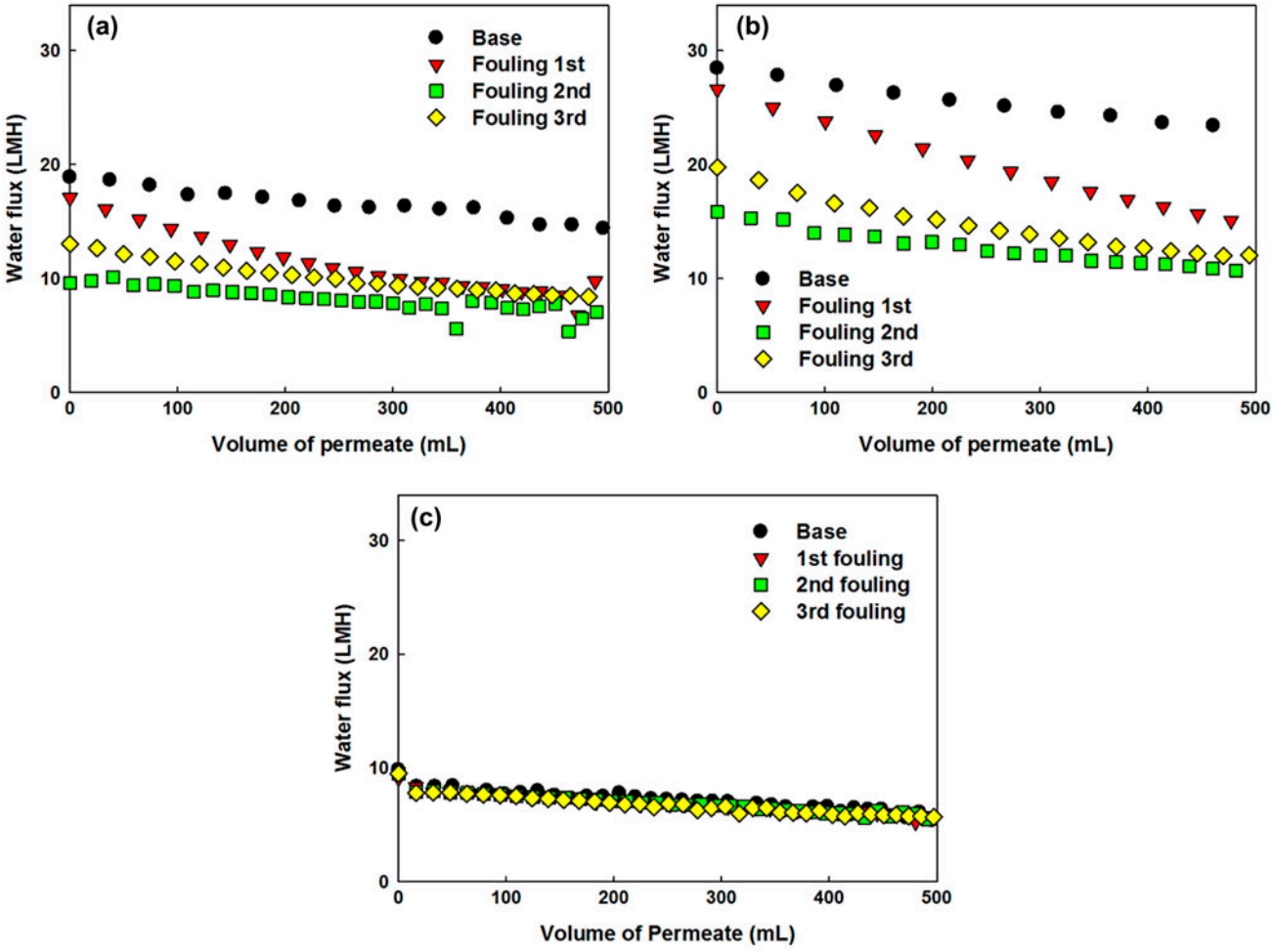

Fig. 7. Water flux (J_w) decline curve for the 1st WWTP Ef in the fouling test: (a) membrane I, (b) membrane II, (c) membrane III.

significantly influence the critical flux [34,39,41–45]. Different from membrane III, membrane I and II were thought to be PA-based membranes with higher roughness than CTA membrane. The reason why membrane I had the highest fouling resistance might be due to its lowest initial flux and membrane characteristics. Therefore, the 1st WWTP Ef contained more foulants, causing severe water flux decline, which was not a suitable source of feed water for membrane I or II, but it was suitable for membrane III.

Interestingly, for both membrane I and II, a stable water fluxes parallel to baseline were observed as the water flux was declined due to foulant deposition onto the membrane as shown in Fig. 7. The disparity of stable fluxes between membrane I and II was relatively narrower (around 7–10 LMH for membrane I and II) compared to that of initial fluxes. To understand this phenomenon, it would be helpful to approach it with the concept of limiting flux. From one of the limiting flux-related-models, the surface interaction based model is known to work well with dilute and stable solutions rather than concentrated or unstable solutions. Limiting flux is governed by foulant-fouled membrane interaction rather than foulant-clean-membrane or membrane properties [34,39,46]. In this experiment, because the same feed water was supplied for the fouling test, it was reasonable to expect similar limiting flux between membrane I and II. Although FO membrane is known to have higher fouling resistance, the feed water quality should be a key factor when designing a FO–RO hybrid system.

In this experiment, after the 2nd batch fouling test, physical cleaning was conducted to find out the reversibility of FO membrane. Fouling layer in FO process is known to be loose and sparse due to the absence of hydraulic pressure compared to pressure-driven

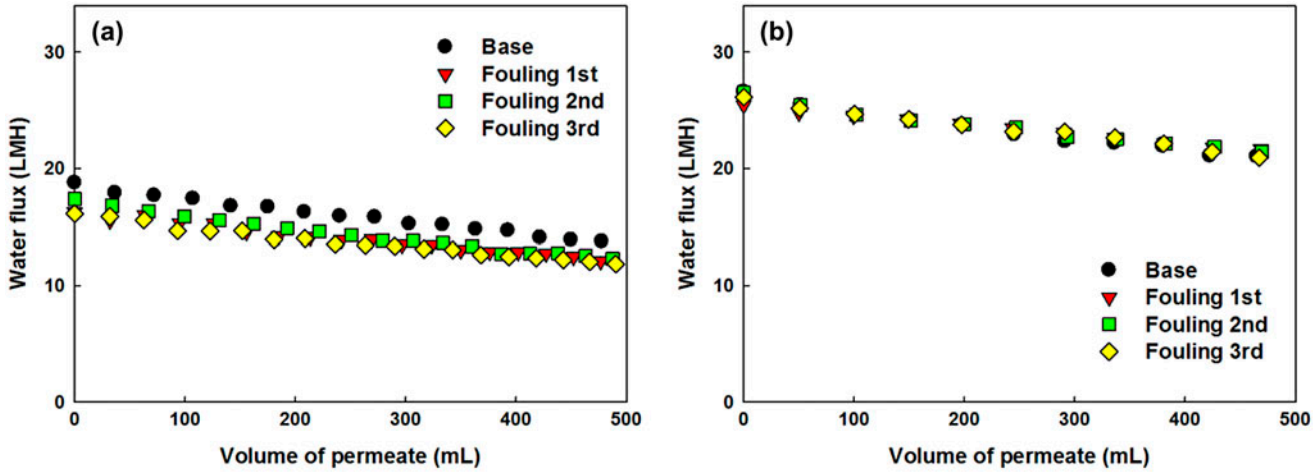

Fig. 8. Water flux (J_w) decline curve for the 2nd WWTP Ef in the fouling test: (a) membrane I, (b) membrane II.

membrane. Around 100% reversibility by physical cleaning has been reported when model colloidal foulant is used [5,47]. However, our results showed a relatively low reversibility (around 70% for both membrane I and II based on initial water flux). Unlike other studies, we used real WWTP Efs as feed water for the FO process. Therefore, various fouling mechanisms might have occurred rather than one. This phenomenon might be attributed to feed water characteristics. The raw WWTP Ef may contain sticky substances such as extracellular polysaccharide (EPS) substances, making fouling layer sticky and compact which could disrupt the efficiency of physical cleaning.

3.3.2.2. 2nd/3rd WWTP Efs. The water flux decline curves for the 2nd and 3rd WWTP Efs are shown in Figs. 8 and 9, respectively. The 2nd and 3rd WWTP Efs contained similar amount of COD, DOC, and UV254. The decline curves for water flux showed similar behaviors when the 2nd and the 3rd WWTP Efs were used as feed water for both membrane I and II. Although membrane II had higher initial flux, the water flux decline of membrane II was negligible, unlike membrane I. In the light of critical flux concept, the foulant-membrane interaction and membrane's chemistry characteristics can significantly affect the critical flux [34,39,41–45]. Since membrane I and II showed the different chemistry characteristics of membrane active layer as shown in Section 3.1.1, this dissimilarity in critical flux might be due to characteristics of the membrane's active layer.

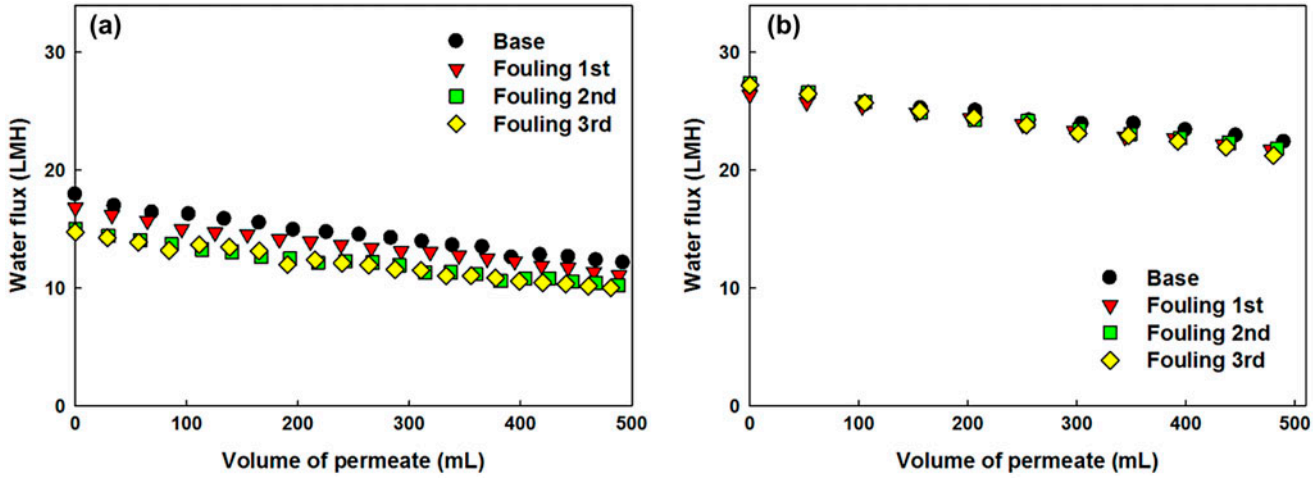

Fig. 9. Water flux (J_w) decline curve for the 3rd WWTP Ef in the fouling test: (a) membrane I, (b) membrane II.

Interestingly, the efficiency of physical cleaning was negligible compared to the case when the 1st WWTP Ef was used as feed water. As shown in Fig. 5, the intensities of region I, II, and IV appeared to be increased to a certain degree after biological treatment. SMP and aromatic protein substances produced during biological process are known to be able to significantly influence membrane fouling more than NOM substances [48,49]. In addition, it has been reported that SMP concentration is proportional to fouling irreversibility in the MBR process [50]. Considering these previous results, SMP and aromatic protein contained in the 2nd and 3rd WWTP Efs might have caused irreversible fouling. Therefore, the degree of irreversibility in the 2nd and 3rd WWTP Efs was higher than that of the 1st WWTP Ef.

4. Conclusions

This study demonstrated the FO membrane characteristics and its performance by the type of FO membranes and feed water quality. Three FO membranes used for this study had different characteristics with different water flux, fouling propensity, and reversibility. When choosing FO membrane with high water flux for the FO–RO hybrid process, it is essential to consider the intrinsic membrane parameters because water flux changes depending on operating condition, such as dilution factor and osmotic pressure of feed water in the FO process. Despite high structural parameter, membrane II showed the highest water permeability. In this study, we used real WWTP Ef as feed water for the FO process. In case of the 1st WWTP Ef, severe water flux decline occurred for both membrane I and II except for membrane III. This was attributed to chemistry characteristic and hydrodynamic force of the FO membrane. In case of the 2nd and the 3rd WWTP Efs, no severe water flux decline was developed. The efficiency of physical cleaning was negligible compared to the case of the 1st WWTP Ef. It is thought that SMP and aromatic protein contained in feed water might have caused low reversibility. Our results imply that, to commercialize FO–RO hybrid process and raise its feasibility, FO performance needs to be tested in real conditions using various FO membranes to select the best one under corresponding conditions. In addition, to raise the cleaning efficiency, the method and strategy of chemical cleaning or pretreatment for commercial FO membrane should be optimized considering its chemical resistance and mechanical strength.

Acknowledgments

This research was supported in part by a grant (code 15IFIP-B088091-02) from Industrial Facilities & Infrastructure Research Program funded by Ministry of Land, Infrastructure and Transport of the Korean government. This work is also supported in part by Korea Ministry of Environment (MOE) as Knowledge-based environmental service (Waste to energy recycling, Ecodesign) Human resource development Project.

References

[1] V. Yangali-Quintanilla, Z. Li, R. Valladares, Q. Li, G. Amy, Indirect desalination of Red Sea water with forward osmosis and low pressure reverse osmosis for water reuse, Desalination 280 (2011) 160–166.
[2] G.W. Intelligence, Desalination Markets 2005–2015: A Global Assessment and Forecast, Media Analytics, Oxford, UK, 2004.
[3] M. Molinos-Senante, F. Hernández-Sancho, R. Sala-Garrido, Economic feasibility study for wastewater treatment: A cost–benefit analysis, Sci. Total Environ. 408 (2010) 4396–4402.
[4] L.F. Greenlee, D.F. Lawler, B.D. Freeman, B. Marrot, P. Moulin, Reverse osmosis desalination: Water sources, technology, and today's challenges, Water Res. 43 (2009) 2317–2348.
[5] S. Lee, C. Boo, M. Elimelech, S. Hong, Comparison of fouling behavior in forward osmosis (FO) and reverse osmosis (RO), J. Membr. Sci. 365 (2010) 34–39.
[6] T.Y. Cath, Osmotically and thermally driven membrane processes for enhancement of water recovery in desalination processes, Desalin. Water Treat. 15 (2012) 279–286.
[7] A. Water, A Novel Hybrid Forward Osmosis Process for Drinking Water Augmentation using Impaired Water and Saline Water Sources, 2009.
[8] V. Yangali-Quintanilla, L. Olesen, J. Lorenzen, C. Rasmussen, H. Laursen, E. Vestergaard, K. Keiding, Lowering desalination costs by alternative desalination and water reuse scenarios, Desalin. Water Treat. 55 (2014) 2437–2445.
[9] G. Blandin, A.R.D. Verliefde, C.Y. Tang, P. Le-Clech, Opportunities to reach economic sustainability in forward osmosis–reverse osmosis hybrids for seawater desalination, Desalination 363 (2015) 26–36.
[10] Y. Xu, X. Peng, C.Y. Tang, Q.S. Fu, S. Nie, Effect of draw solution concentration and operating conditions on forward osmosis and pressure retarded osmosis performance in a spiral wound module, J. Membr. Sci. 348 (2010) 298–309.
[11] N.T. Hancock, P. Xu, D.M. Heil, C. Bellona, T.Y. Cath, Comprehensive bench-and pilot-scale investigation of trace organic compounds rejection by forward osmosis, Environ. Sci. Technol. 45 (2011) 8483–8490.
[12] M. Park, J. Lee, C. Boo, S. Hong, S.A. Snyder, J.H. Kim, Modeling of colloidal fouling in forward osmosis membrane: Effects of reverse draw solution permeation, Desalination 314 (2013) 115–123.

[13] C.Y. Tang, Q. She, W.C.L. Lay, R. Wang, A.G. Fane, Coupled effects of internal concentration polarization and fouling on flux behavior of forward osmosis membranes during humic acid filtration, J. Membr. Sci. 354 (2010) 123–133.
[14] N.T. Hancock, T.Y. Cath, Solute coupled diffusion in osmotically driven membrane processes, Environ. Sci. Technol. 43 (2009) 6769–6775.
[15] Y.C. Kim, S.-J. Park, Experimental study of a 4040 spiral-wound forward-osmosis membrane module, Environ. Sci. Technol. 45 (2011) 7737–7745.
[16] A. Tiraferri, N.Y. Yip, A.P. Straub, S. Romero-Vargas Castrillon, M. Elimelech, A method for the simultaneous determination of transport and structural parameters of forward osmosis membranes, J. Membr. Sci. 444 (2013) 523–538.
[17] R.J. Petersen, Composite reverse-osmosis and nanofiltration membranes, J. Membr. Sci. 83 (1993) 81–150.
[18] C. Tang, Y. Kwon, J. Leckie, Probing the nano- and micro-scales of reverse osmosis membranes—A comprehensive characterization of physiochemical properties of uncoated and coated membranes by XPS, TEM, ATR-FTIR, and streaming potential measurements, J. Membr. Sci. 287 (2007) 146–156.
[19] F. Lotfi, Membrane fouling during fertiliser drawn forward osmosis desalination using brackish groundwater, Diss. (2013).
[20] N.Y. Yip, A. Tiraferri, W.A. Phillip, J.D. Schiffman, M. Elimelech, High performance thin-film composite forward osmosis membrane, Environ. Sci. Technol. 44 (2010) 3812–3818.
[21] W.W. Ho, K.K. Sirkar, Membrane Handbook, Springer Science & Business Media, 1992.
[22] V. Freger, J. Gilron, S. Belfer, TFC polyamide membranes modified by grafting of hydrophilic polymers: An FT-IR/AFM/TEM study, J. Membr. Sci. 209 (2002) 283–292.
[23] A.I. Schäfer, A.G. Fane, T.D. Waite, Nanofiltration: Principles and Applications, Elsevier, 2005.
[24] V. Parida, H.Y. Ng, Forward osmosis organic fouling: Effects of organic loading, calcium and membrane orientation, Desalination 312 (2013) 88–98.
[25] R.K. Henderson, A. Baker, K.R. Murphy, A. Hambly, R.M. Stuetz, S.J. Khan, Fluorescence as a potential monitoring tool for recycled water systems: A review, Water Res. 43 (2009) 863–881.
[26] S.-J. Kim, B.S. Oh, H.-W. Yu, L.H. Kim, C.-M. Kim, E.-T. Yang, M.S. Shin, A. Jang, M.H. Hwang, I.S. Kim, Foulant characterization and distribution in spiral wound reverse osmosis membranes from different pressure vessels, Desalination 370 (2015) 44–52.
[27] W. Chen, P. Westerhoff, J.A. Leenheer, K. Booksh, Fluorescence excitation-emission matrix regional integration to quantify spectra for dissolved organic matter, Environ. Sci. Technol. 37 (2003) 5701–5710.
[28] W. Chen, P. Westerhoff, J.A. Leenheer, K. Booksh, Fluorescence excitation−emission matrix regional integration to quantify spectra for dissolved organic matter, Environ. Sci. Technol. 37 (2003) 5701–5710.
[29] S. Hong, M. Elimelech, Chemical and physical aspects of natural organic matter (NOM) fouling of nanofiltration membranes, J. Membr. Sci. 132 (1997) 159–181.
[30] A. Achilli, T.Y. Cath, A.E. Childress, Power generation with pressure retarded osmosis: An experimental and theoretical investigation, J. Membr. Sci. 343 (2009) 42–52.
[31] T. Nguyen, F.A. Roddick, L. Fan, Biofouling of water treatment membranes: a review of the underlying causes, monitoring techniques and control measures, Membranes 2(4) (2012) 804–840.
[32] X. Zhu, M. Elimelech, Colloidal fouling of reverse osmosis membranes: Measurements and fouling mechanisms, Environ. Sci. Technol. 31 (1997) 3654–3662.
[33] X. Zhu, M. Elimelech, Fouling of reverse osmosis membranes by aluminum oxide colloids, J. Environ. Eng. 121 (1995) 884–892.
[34] C.Y. Tang, T. Chong, A.G. Fane, Colloidal interactions and fouling of NF and RO membranes: A review, Adv. Colloid Interface Sci. 164 (2011) 126–143.
[35] C.Y. Tang, Y.-N. Kwon, J.O. Leckie, Characterization of humic acid fouled reverse osmosis and nanofiltration membranes by transmission electron microscopy and streaming potential measurements, Environ. Sci. Technol. 41 (2007) 942–949.
[36] R. Field, D. Wu, J. Howell, B. Gupta, Critical flux concept for microfiltration fouling, J. Membr. Sci. 100 (1995) 259–272.
[37] C.Y. Tang, Y.-N. Kwon, J.O. Leckie, Fouling of reverse osmosis and nanofiltration membranes by humic acid—Effects of solution composition and hydrodynamic conditions, J. Membr. Sci. 290 (2007) 86–94.
[38] R.D. Cohen, R. Probstein, Colloidal fouling of reverse osmosis membranes, J. Colloid Interface Sci. 114 (1986) 194–207.
[39] C.Y. Tang, J.O. Leckie, Membrane independent limiting flux for RO and NF membranes fouled by humic acid, Environ. Sci. Technol. 41 (2007) 4767–4773.
[40] C.Y. Tang, Y.-N. Kwon, J.O. Leckie, The role of foulant–foulant electrostatic interaction on limiting flux for RO and NF membranes during humic acid fouling—Theoretical basis, experimental evidence, and AFM interaction force measurement, J. Membr. Sci. 326 (2009) 526–532.
[41] T. Chong, F. Wong, A. Fane, Enhanced concentration polarization by unstirred fouling layers in reverse osmosis: Detection by sodium chloride tracer response technique, J. Membr. Sci. 287 (2007) 198–210.
[42] D. Kwon, S. Vigneswaran, A. Fane, R.B. Aim, Experimental determination of critical flux in cross-flow microfiltration, Sep. Purif. Technol. 19 (2000) 169–181.
[43] P. Neal, H. Li, A. Fane, D. Wiley, The effect of filament orientation on critical flux and particle deposition in spacer-filled channels, J. Membr. Sci. 214 (2003) 165–178.
[44] I.H. Huisman, E. Vellenga, G. Trägårdh, C. Trägårdh, The influence of the membrane zeta potential on the critical flux for crossflow microfiltration of particle suspensions, J. Membr. Sci. 156 (1999) 153–158.
[45] S. Kim, H. Park, Applicability assessment of subcritical flux operation in crossflow microfiltration with a concentration polarization model, J. Environ. Eng. 128 (2002) 335–340.
[46] Q. She, C.Y. Tang, Y.-N. Wang, Z. Zhang, The role of hydrodynamic conditions and solution chemistry on protein fouling during ultrafiltration, Desalination 249 (2009) 1079–1087.
[47] C. Boo, S. Lee, M. Elimelech, Z. Meng, S. Hong, Colloidal fouling in forward osmosis: Role of reverse salt diffusion, J. Membr. Sci. 390–391 (2012) 277–284.

[48] E.-C. Polysaccharides, Soluble Microbial Products, and Natural Organic Matter Impact on Nanofiltration Membranes Flux Decline Fonseca, A. Cristina; Summers, R. Scott; Greenberg, Alan R.; Hernandez, Mark T., Environ. Sci. Technol. 41 (2007) 2491–2497.
[49] H. Yu, F. Qu, H. Chang, S. Shao, X. Zou, G. Li, H. Liang, Understanding ultrafiltration membrane fouling by soluble microbial product and effluent organic matter using fluorescence excitation–emission matrix coupled with parallel factor analysis, Int. Biodeterior. Biodegrad. 102 (2015) 56–63.
[50] M. Yao, B. Ladewig, K. Zhang, Identification of the change of soluble microbial products on membrane fouling in membrane bioreactor (MBR), Desalination 278 (2011) 126–131.